


## Polarization switching of segmentally helical undulators in a diffraction-limited storage ring

Nanrui Yang<sup>1</sup>, Yuanfang Xu<sup>1</sup>, Zhouyu Zhao<sup>1,\*</sup> and Heting Li

*National Synchrotron Radiation Laboratory, University of Science and Technology of China, Hefei, 230029, Anhui, People's Republic of China*

 (Received 18 March 2023; accepted 7 August 2023; published 17 August 2023)

Polarization switching of synchrotron radiation has wide application prospects in various areas, requiring a high switching frequency between horizontally linear polarization (HLP) and vertically linear polarization (VLP) or between left-hand circular polarization (LCP) and right-hand circular polarization (RCP). To make it possible for realizing a fast polarization switching, in this paper we simplify and incorporate the previous schemes based on segmentally helical undulators connected by phase shifters. Adjacent undulators are set by the same or opposite polarization state to generate circularly or linearly polarized radiation. Theoretical analysis and simulations for radiation characteristics are reported in details. By combining the polarization adjustment of each helical undulator with the phase shifters, both the switching for HLP/VLP and LCP/RCP can be realized in the same undulator scheme. The on-axis heat load can always be effectively suppressed. Benefiting from the extremely low emittance and taking into account the space occupied by phase shifters, the proposed scheme shows a significant advantage in preserving the photon flux with a high polarization degree in a diffraction limited storage ring compared with a typical third generation storage ring. In addition, we also study the influence of beam deviation at each undulator segment, the segment number limited by the practical length of straight section and the issues related to user experiments.

DOI: [10.1103/PhysRevAccelBeams.26.080701](https://doi.org/10.1103/PhysRevAccelBeams.26.080701)

### I. INTRODUCTION

Polarization control of undulator radiation has attracted wide attention due to its great application prospects in various areas. In the storage ring light sources, several types of undulators have been developed to realize arbitrary polarization states, such as APPLE-II [1,2], APPLE-X and DELTA [3–5] undulators. FIGURE-8 [6,7], APPLE-KNOT [8,9], and DELTA-AMPU [10,11] undulators have been further proposed or put into practice to reduce the on-axis heat load. In general, the polarization state of the pure-permanent-magnet undulator can be easily tuned by shifting the magnet array mechanically. The ultimate limit of the polarization switching frequency is smaller than the level of Hz. However, there is still a strong demand to improve the switching frequency of the polarization state. For example, detecting the spin and orbital moment of a material in x-ray magnetic linear/circular dichroism (XMLD/XMCD) requires a high switching frequency between horizontally linear polarization (HLP) and vertically linear polarization

(VLP) or between left-hand circular polarization (LCP) and right-hand circular polarization (RCP).

To obtain a high switching frequency, various methods have been proposed or put into practice, such as electromagnetic switching [12,13], photon beam line switching [14,15], electron beam orbit switching [16–18], and nature close orbit switching [19]. However, these methods face different defects, including a heavy disturbance on the storage ring, different photon beam lines and the other technical issues, thus cannot realize a high switching frequency in the normal operation mode of storage ring.

Cross-planar undulators have been initially demonstrated to generate circularly polarized radiation based on the field superposition between HLP and VLP radiation in the storage ring light sources [20–22] and free-electron lasers [23–29]. The polarization state is switched by swapping the phase shift. The switching induced longitudinal mismatch has little influence on the storage ring, and the orbit bump and distortion induced from the phase shifter are quite small, thus a much higher switching frequency can be expected. However, in the typical two crossed undulators, the polarization degree is greatly degenerated and the on-axis heat load also cannot be suppressed. In the past few years, two kinds of segmentally helical undulator schemes have been proposed [30–36]. One is able to obtain linearly polarized radiation by setting each helical undulator with the opposite polarization state to its adjacent segments.

\*yuzz@ustc.edu.cn

*Published by the American Physical Society under the terms of the Creative Commons Attribution 4.0 International license. Further distribution of this work must maintain attribution to the author(s) and the published article's title, journal citation, and DOI.*

By optimizing the phase shifts, linearly polarized radiation can be flexibly tuned with an arbitrarily polarized direction. The on-axis heat load is always effectively suppressed. Another scheme is already an idea which is made for an upgrade plan for SPring-8 [34,37]. It utilizes two helical undulator segmentations with the opposite polarization states. Each helical undulator in one segmentation is the same. One undulator segmentation is able to generate spectrum split on the axis, while another segmentation with the opposite polarization state is optimized as a single helical undulator. The undulator radiation can be switched between LCP and RCP by alternately changing the phase shifts. However, in a typical third generation storage ring, due to a large emittance and a large beam size, these schemes have difficulty overcoming a sharp reduction in flux or polarization degree, especially for the second scheme.

The well-known diffraction-limited storage ring (DLSR) [38,39] can reduce the emittance by 1-2 orders of magnitude smaller than before, and obtain a small beam size. Most of the resonant photon flux is focused on the axis, thus the reduction in flux or polarization degree of the segmental undulator scheme can be greatly relieved. The previous work requires the delicate control of phase shifter to obtain arbitrarily linear polarization. Actually, in the fast switching of linear polarization, HLP and VLP are adequate for most of the relevant user experiments. In this paper, these two segmental undulator schemes [32,34] are simplified and merged into a same undulator scheme. Combining the polarization adjustment of each helical undulator with the optimizations of phase shifters and monochromator, both the switching of HLP/VLP and LCP/RCP can be realized with a considerable photon flux and a relatively high polarization degree in a DLSR. In general, the switching frequency with dozens of Hz can be expected by using the electromagnet phase shifter in this scheme. It is also possible to be further improved if the induced beam bump coupled with the eddy current can be well controlled. The on-axis heat load is always effectively suppressed. The rest of this paper is organized as follows: First, the theoretical analysis is given based on an ideal electric field model. The radiation performance with different phase shifts and segments is studied in details. Then we compare the radiation performance between a DLSR and a typical third generation storage ring. In addition, the influence of beam deviation is studied based on the electron radiation model, which is given in the Appendix. A thoughtful discussion is also made, focusing on the segment number limited by the practical length of straight section, the specific issues related to user experiments and the polarization switching frequency. Finally we make a summary.

## II. PRINCIPLE

To illustrate the basic principle of the proposed helical undulator scheme, in the following we introduce an ideal

electric field model. The electron radiation model in the Appendix is used to accurately calculate the radiation performance under some specific situations.

In the electron storage ring, the radiation electric field from the planar undulator can be simplified as an  $N$ -cycle cosine wave ( $N \gg 1$ ). The frequency spectrum of electric field around the fundamental frequency is obtained by Fourier transformation

$$E_f(\omega) = E_0 \int_{-\frac{T}{2}}^{\frac{T}{2}} \cos(\omega_1 t) e^{-i\omega t} dt \approx \frac{E_0 T}{2} \text{sinc} \left[ (\omega - \omega_1) \frac{T}{2} \right], \quad (1)$$

where  $E_0$  is the amplitude of the electric field,  $\omega_1$  is the fundamental frequency,  $T = 2\pi N/\omega_1$  is the time duration of radiation, and  $N$  is the undulator period number. Under the given undulator strength parameter  $K$  and Lorentz factor of electron  $\gamma$ ,  $\omega_1$  depends on the observation angle  $\theta$  as

$$\omega_1(\theta) = \omega_1(0) \frac{1 + K^2}{1 + K^2 + \gamma^2 \theta^2}. \quad (2)$$

For a helical undulator, the magnetic field can be decomposed to two mutually orthogonal components in the horizontal and vertical direction with a constant phase difference ( $\pi/2$ ). The electric field of LCP/RCP radiation in time domain is simplified as

$$\begin{aligned} \mathbf{E}(t) &= \mathbf{E}_x(t) + \mathbf{E}_y(t) \\ &= E_0 \cos(\omega_1 t) \mathbf{e}_x \pm E_0 \sin(\omega_1 t) \mathbf{e}_y. \end{aligned} \quad (3)$$

Assume an undulator scheme is composed of  $M$  segments with the same undulator parameter and the adjustable phase shifter  $\Delta T_m$  between the ( $m$ )th and ( $m-1$ )th segments. Here  $\Delta T_1$  is the phase shift before the first segment and is set to zero. The frequency spectrum can be deduced as

$$\mathbf{E}(\omega) = \sum_{m=1}^M \int_{-\frac{T}{2}}^{\frac{T}{2}} \mathbf{E}_m(t) e^{-i\omega[t+(m-1)T+\sum_{m=1}^M \Delta T_m]} dt. \quad (4)$$

Then the whole energy spectrum is calculated as

$$\begin{aligned} I(\omega) &= I_x(\omega) + I_y(\omega) \\ &= |\mathbf{E}_x(\omega)|^2 + |\mathbf{E}_y(\omega)|^2. \end{aligned} \quad (5)$$

First, let us consider the case of each helical undulator segment having an opposite polarization state to its adjacent segments, as shown in Fig. 1(a). LCP and RCP undulators are alternately arrayed with the same phase shift ( $\Delta\varphi_m = \omega_1 \Delta T_m = \Delta\varphi, m \geq 2$ ) between them. According to the equations above, we have the energy spectrum

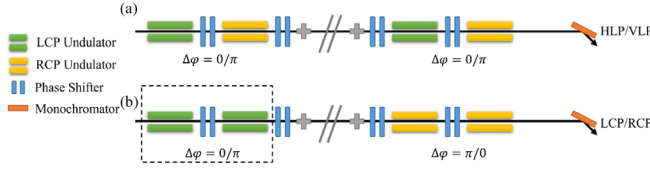


FIG. 1. Polarization control and switching of (a) HLP/VLP radiation and (b) LCP/RCP radiation at segmentally helical undulators.

$$I_x(\omega) = E_f^2(\omega) \frac{\sin^2[M\omega(\Delta T + T)/2]}{\sin^2[\omega(\Delta T + T)/2]}, \quad (6)$$

$$I_y(\omega) = E_f^2(\omega) \frac{\sin^2[M\omega(\Delta T + T)/2]}{\cos^2[\omega(\Delta T + T)/2]}, \quad (M = \text{even})$$

or

$$= E_f^2(\omega) \frac{\cos^2[M\omega(\Delta T + T)/2]}{\cos^2[\omega(\Delta T + T)/2]}, \quad (M = \text{odd}) \quad (7)$$

with

$$E_x(\omega) = E_f(\omega) \frac{1 - e^{-i\omega M(\Delta T + T)}}{1 - e^{-i\omega(\Delta T + T)}}, \quad (8)$$

$$E_y(\omega) = \frac{E_f(\omega)}{i} \frac{1 \mp e^{-i\omega M(\Delta T + T)}}{1 + e^{-i\omega(\Delta T + T)}}. \quad (9)$$

Particularly, if  $M$  is an even number,  $I(\omega)$  can be described as

$$I(\omega)_{\text{opposite}} = 4E_f^2(\omega) \frac{\sin^2[M(2\pi N + \Delta\varphi)\omega/2\omega_1]}{\sin^2[(2\pi N + \Delta\varphi)\omega/\omega_1]} \quad (10)$$

with

$$E_y(\omega) = E_x(\omega) \frac{1 - \cos[(2\pi N + \Delta\varphi)\omega/\omega_1]}{\sin[(2\pi N + \Delta\varphi)\omega/\omega_1]} = E_x \tan \psi, \quad (11)$$

where  $\psi$  is  $(2\pi N + \Delta\varphi)\omega/2\omega_1$ .

This indicates that  $E_x(\omega)$  and  $E_y(\omega)$  have the same phase. Circularly polarized radiation is effectively canceled, and then linearly polarized radiation is generated. The polarization angle  $\psi$  is determined by Eq. (11). For the fundamental frequency on the axis,  $\psi$  is fully dependent on  $\Delta\varphi$ . If  $\Delta\varphi$  is 0 or the even multiple of  $\pi$ ,  $\tan \psi$  equals 0 which means that the radiation is horizontally polarized. If  $\Delta\varphi$  is the odd multiple of  $\pi$ ,  $\tan \psi$  is infinity, then vertically polarized radiation can be obtained. The polarization angle increases linearly from  $0^\circ$  (horizontal) to  $90^\circ$  (vertical) with  $\Delta\varphi$  increasing from 0 to  $\pi$ , while the on-axis energy spectrum achieves the maximum at  $0^\circ$  and  $90^\circ$  polarization

angle. The switching of HLP/VLP radiation can be realized by swapping the phase shifts.

In addition, according to Eq. (10), we can find that the energy spectrum at  $\omega = \omega_1$  vanishes if  $\Delta\varphi$  equals  $2\pi/M$  and  $M \geq 4$  ( $M$  is an even number). In fact, here the photon flux does not fully vanish, but is spatially diffused. At the fixed observation frequency of  $\omega_1(0)$ , the right fraction of  $I(\omega)$  becomes an approximately periodic wave depending on  $\omega_1(\theta)$ . The peak flux density is distributed within the angular width of the first oscillation period  $\Delta\theta_w$ , which can be described as

$$\Delta\theta_w = \frac{1}{\gamma} \sqrt{\frac{1 + K^2}{MN + 1}} < \frac{1}{\gamma} \sqrt{\frac{1 + K^2}{MN}} = 2\sigma'_r, \quad (12)$$

where  $\sigma'_r$  is the diffraction angle.

Let us further consider the case in which each undulator segment is identical and has the same polarization state,  $E_x(\omega)$  and  $I_x(\omega)$  will be the same as in Eqs. (8) and (6), respectively. In this condition,  $E_y(\omega)$  equals  $-iE_x(\omega)$  and  $I_y(\omega)$  is the same as  $I_x(\omega)$ . Different from the former case, the polarization state in this case is the same as that of the single helical undulator. The whole energy spectrum can be given as

$$I(\omega)_{\text{identical}} = 2E_f^2(\omega) \frac{\sin^2[M(2\pi N + \Delta\varphi)\omega/2\omega_1]}{\sin^2[(2\pi N + \Delta\varphi)\omega/2\omega_1]} = 2\cos^2[(2\pi N + \Delta\varphi)\omega/2\omega_1] I(\omega)_{\text{opposite}}. \quad (13)$$

Assuming an undulator scheme consisting of  $2M$  helical undulators, as shown in Fig. 1(b). The first  $M$  segments are LCP undulators and the second  $M$  segments are RCP undulators. We can find that the on-axis energy spectrum also vanishes at  $\omega = \omega_1$  if  $\Delta\varphi$  equals to  $2\pi/M$ , in which most of the flux is spatially diffused. In this condition, with the decrease of the slit width, the received flux will be sharply reduced. The on-axis energy spectrum achieves the maximum at the phase shift of 0 or  $2\pi$ . If the phase shifts between LCP/RCP undulators are set to 0 while the phase shifts between other RCP/LCP undulators are set to  $2\pi/M$ , RCP/LCP radiation has little flux on the axis and LCP/RCP radiation can be collected. To fully filter the RCP/LCP radiation and obtain a high polarization degree for the LCP/RCP radiation, the slit width should be reduced to some extent, which will cause an inevitable reduction in flux. Obviously, LCP and RCP radiation can also be switched when we swap the phase shifts. Specifically, in a same segmentally helical undulator scheme, the effective undulator length of the identical case is half of the opposite case, thus the photon flux in identical case should be smaller than that in opposite case.

### III. BASIC RADIATION PERFORMANCE

In this paper, the radiation performances are mainly simulated by *SPECTRA* [40]. The parameters used in simulations are given in Table I, which are referenced to the Hefei Advanced Light Facility (HALF), a 2.2 GeV DLSR developed by the National Synchrotron Radiation Laboratory in China [41,42]. The natural emittance is about 100 pm rad. The target photon energy is selected at 700 eV, where the edges of several kinds of rare earth elements locate around. The undulator period length is set to 41 mm and the strength parameter  $K$  is set to 0.776. The period number per segment  $N = 20$  is preliminarily chosen with four helical undulator segments, and three 0.2-m-long phase shifters placed between them. The total space occupied by this scheme is near 4 m. The polarization state of each segment can be mechanically adjusted from LCP to RCP.

#### A. Polarization switching

For the opposite case, each helical undulator segment is set with an opposite polarization state to its adjacent segments. As shown in Fig. 1(a), linearly polarized radiation is realized by the superposition between LCP and RCP radiation. Following the theoretical analysis given in the above section, the phase shifts  $\Delta\varphi$  are alternately switched between 0 and  $\pi$  to generate HLP and VLP, respectively. The flux is reduced by approximately half in the above progress, nevertheless, a helical undulator generates a higher flux than a planar undulator. The total flux in this linear mode will be close to a planar undulator.

The flux and polarization degree for HLP/VLP are shown in Fig. 2. Under the same acceptance angle, these two different linear modes have the same flux and polarization degree. The angular divergence  $\sigma_p$  is defined as Eq. (A3) in the Appendix. The flux increases from  $6.5 \times 10^{14}$  to  $1.7 \times 10^{15}$  when the acceptance angle increases from  $1\sigma_p$  to  $2\sigma_p$ , but the polarization degree decreases from 93.2% to 76.8%. Note that here the flux is after passing through the monochromator at the energy with the highest polarization degree. Most of the on-axis flux can be collected within the acceptance angle of  $2\sigma_p$ . To make a direct comparison between the proposed scheme and the

TABLE I. Parameters used in simulations.

Parameter	Specification	Unit
Period number per segment $N$	20/10/5	...
Segment number $M$	4/8/16	...
Period length	41	mm
Undulator strength parameter $K$	0.776	...
Photon energy	700	eV
Electron energy	2.2	GeV
Average current	500	mA
Natural emittance	100	pm rad

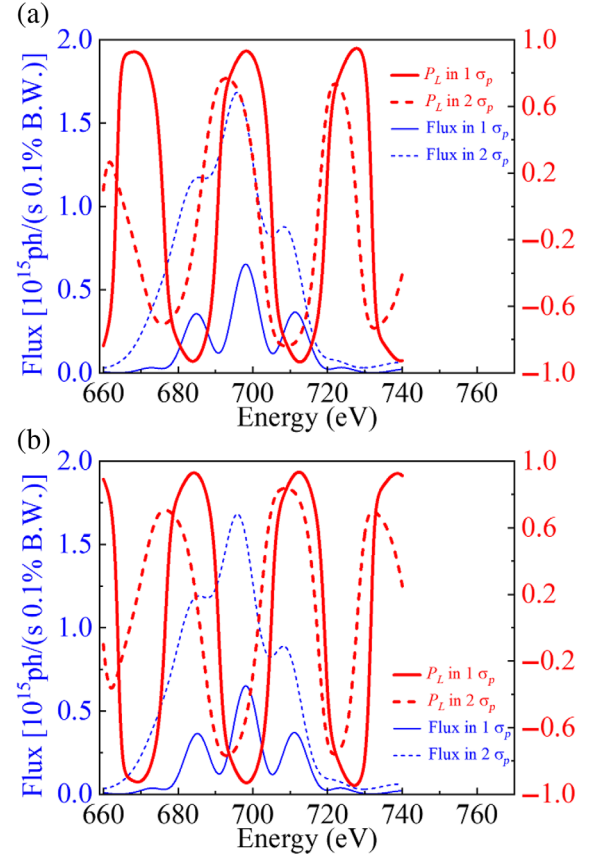


FIG. 2. Photon flux and polarization degree for (a) HLP radiation and (b) VLP radiation.

conventional planar undulator, a single long undulator ( $4 \times 0.82$  m) is taken as the reference. When the acceptance angle increases from  $1\sigma_p$  to  $2\sigma_p$ , the flux increases from  $1.0 \times 10^{15}$  to  $2.3 \times 10^{15}$  while the polarization degree remains above 99%. The flux of the proposed scheme is about 35% less than a planar undulator and a considerable polarization degree can still be obtained.

Compared with linear polarization switching, circular polarization switching is also achieved by the superposition of circularly polarized radiation, however, superposition occurs in undulators with the identical polarization state. As shown in Fig. 1(b), it contains  $2M$  undulators, in which the first  $M$  undulators are set with LCP/RCP while the last  $M$  undulators are set with RCP/LCP. To keep the same layout as the opposite case, here  $M$  should be set to 2. The radiation superposition from  $M$  undulators is strengthened and the radiation in another  $M$  undulators is canceled on the axis. The phase shifts  $\Delta\varphi$  are alternately switched between 0,  $\pi$  and  $\pi$ , 0 to generate LCP and RCP, respectively. Since the identical case only has half the effective undulator length, both the flux and polarization degree in identical cases should be smaller than those in opposite cases.

The flux and polarization degree for LCP/RCP are shown in Fig. 3. For LCP, when the acceptance angle increases from  $1\sigma_p$  to  $2\sigma_p$ , the flux increases from  $4.2 \times 10^{14}$  to  $1.5 \times 10^{15}$ ,

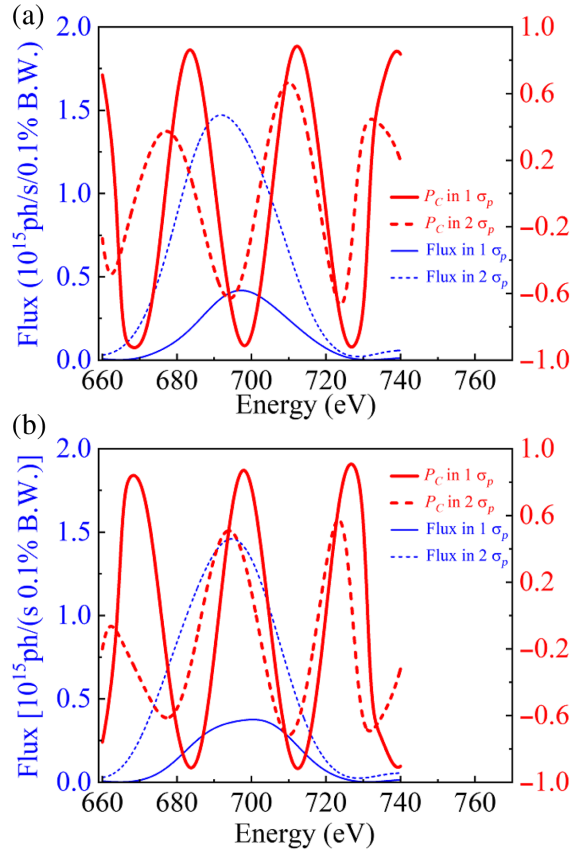


FIG. 3. Photon flux and polarization degree for (a) LCP radiation and (b) RCP radiation.

but the polarization degree decreases from 91.3% to 62.9%. For RCP, the flux increases from  $3.8 \times 10^{14}$  to  $1.5 \times 10^{15}$ , and the polarization degree decreases from 87.1% to 50.9%. Polarization degree decreases sharply with increasing acceptance angle, which comes from the imperfect off-axis counteraction of radiation fields between undulator segments with  $\Delta\varphi = \pi$ . RCP achieves almost the same flux as LCP, but has a lower polarization degree. Such a difference in polarization degree is caused by the space occupied by phase shifters and the sequence between LCP and RCP undulators. If we utilize the ideal phase shifts without actual space, this difference will be reduced. In addition, we can find that both the flux and polarization degree in the circular mode are indeed smaller than those in the linear mode. We also compare the circular mode with a single helical undulator. By matching the phase shifts and adjusting the undulators to the same polarization state, the entire scheme is equivalent to a single long helical undulator. When the acceptance angle increases from  $1\sigma_p$  to  $2\sigma_p$ , the flux increases from  $1.3 \times 10^{15}$  to  $2.9 \times 10^{15}$  while the polarization degree remains above 99%. Within  $1\sigma_p$  acceptance angle, the flux is reduced by approximately 3 times compared to the conventional undulator, and the polarization degree is reduced to 91%. Within  $2\sigma_p$  acceptance angle, the flux is reduced by 2 times

compared to the conventional undulator, but the polarization degree is significantly reduced.

In general, the linear mode can achieve a better performance than the circular mode. Compared with the conventional undulator, the linear mode still has the considerable flux and polarization degree, while in the circular mode the polarization degree is greatly reduced. To obtain a considerable polarization degree, the acceptance angle in the circular mode must be narrowed, that is, on the sacrifice of received flux. Actually, the obtained polarization degree and flux in this scheme are already possible to satisfy most of the relevant experiments. Another notable merit is the on-axis heat load suppression. In a typical planar undulator, a heavy heat load can be found on the axis, especially for resonating at a low photon energy in a high-energy storage ring. In the proposed scheme, both linear and circular polarized radiation are realized by the helical undulator. The on-axis heat load can be reduced by nearly an order of magnitude compared to a planar undulator.

## B. Undulator segments

We have demonstrated the radiation performance with four undulator segments. Actually, under the same total period number, increasing the segment number is beneficial to improving the polarization degree or increasing the flux under the same polarization degree [32,34]. In the following, the segment configuration is changed from  $4 \times 20$  to  $8 \times 10$ ,  $16 \times 5$ . Here we only limit ourselves in the case of a constant total period number, without taking into account the actual space of a given straight section. We will make a specific discussion with the limitation of actual space at HALF in Sec. VI.

First, we increase the segment number to 8. The flux of the linear mode is always greater than that of the circular mode, as shown in Fig. 4. With the increase of acceptance angle, both  $P_L$  of the linear mode and  $P_C$  of the circular mode are decreased. For the polarization degree, the

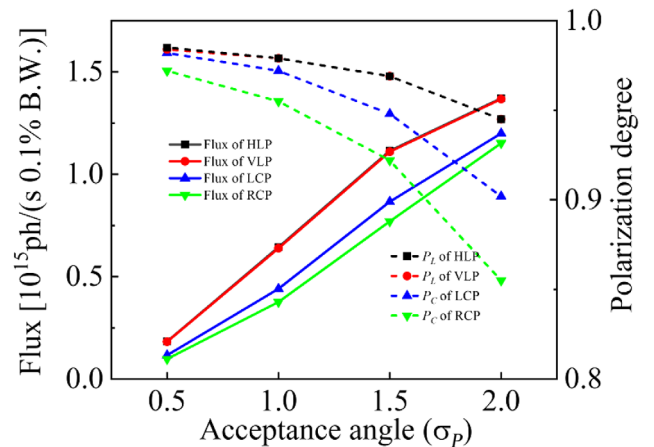


FIG. 4. Radiation performances depend on the acceptance angle with 8 segments at 700 eV.

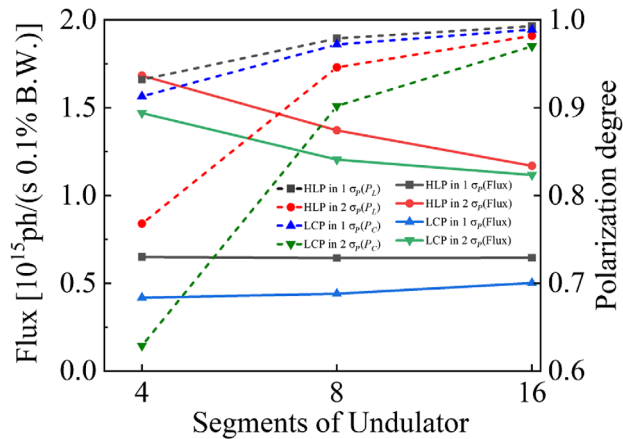


FIG. 5. Radiation performances of HLP and LCP depend on the segment number at 700 eV.

circular mode is more sensitive to the acceptance angle than the linear mode. Within  $1\sigma_p$ , both  $P_L$  and  $P_C$  are greater than 95%. If increasing the acceptance angle to  $2\sigma_p$ ,  $P_L$  can still be maintained above 94% but  $P_C$  is reduced to 85%–90%. Nevertheless, compared with the 4-segment scheme, the polarization degree in the 8-segment scheme is significantly improved. The reduced flux within a large acceptance angle implies that the superposition/counteraction mechanism is strengthened in this 8-segment scheme.

Figure 5 shows the radiation performances depending on different segment numbers. The HLP and LCP radiation are taken as examples. As the segment number increases from 4 to 8, the flux decreases slightly but the polarization degree increases significantly. When we further increase the segment number to 16, the change in polarization degree slows down. The polarization degree can reach a high level under a large number of segments. Even at a large acceptance angle, both  $P_C$  and  $P_L$  can reach 90%, while at a small acceptance angle the polarization degree is always above 97%. However, with the increase of segment number, the number of phase shifters should also be synchronously increased, so the actual space used by undulators will be further reduced. In the case of 16 segments, the required number of phase shifters is up to 15. The segment number should be optimized by a comprehensive consideration of the available space in the straight section, the experimental demand for radiation performance and the evaluation of technical difficulty.

#### IV. THIRD GENERATION STORAGE RING AND DLSR

The above simulation results are based on the parameters of a 2.2 GeV DLSR, in which the divergence angle at 700 eV is basically determined by the diffraction angle. For the third generation storage ring, the electron beam is normally a flat beam and its natural emittance is 1–2 orders of magnitude larger than that of a DLSR. In the following,

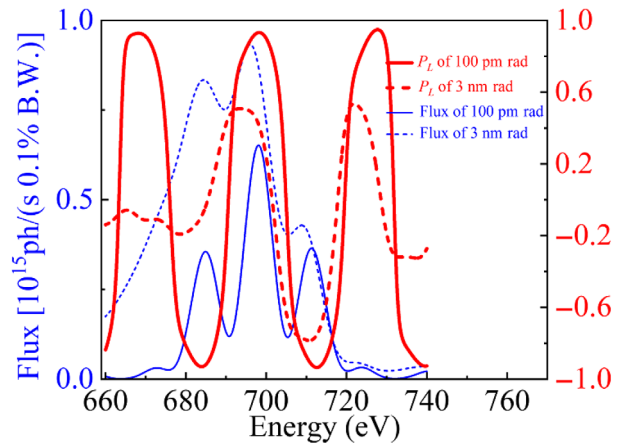


FIG. 6. Radiation performances (HLP) within  $1\sigma_p$  for the third generation storage ring and DLSR.

we also take HLP and LCP as examples to compare the proposed scheme under a small emittance and a large emittance. We only artificially increase the natural emittance from 100 pm rad to 3 nm rad to represent a typical third generation storage ring. To make a clear demonstration of the influence of emittance, the other parameters are the same. Four segments are used here. Note that the angular divergence  $\sigma_p$  is normalized to each case with different emittance, thus, 3 nm rad corresponds to a much larger  $\sigma_p$  than 100 pm rad. As shown in Figs. 6 and 7, with the significant increase of the emittance, the change in the flux is relatively small, but the polarization degree decreases significantly. Within  $1\sigma_p$ , the polarization degrees of HLP and LCP radiation are decreased from 93.2% to 50.7% and from 91.3% to 45.4%, respectively. The unshown simulation results within  $2\sigma_p$  reveal that the corresponding polarization degrees are further decreased from 76.8% to 34.6% and from 62.9% to 26.7%, respectively. Both the HLP and LCP radiation suffer a sharp reduction in polarization degree with increasing emittance. Such a low polarization degree in the third

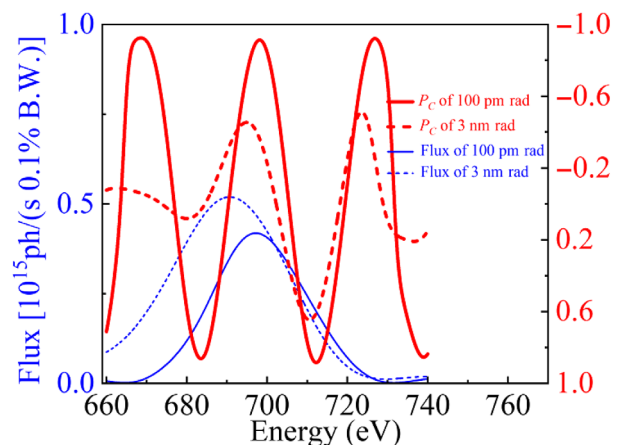


FIG. 7. Radiation performances (LCP) within  $1\sigma_p$  for the third generation storage ring and DLSR.

generation storage ring makes it difficult to satisfy user experiments. Even if the polarization degree can be improved by narrowing the acceptance angle to some extent, the received flux will be greatly reduced. For example, to obtain a same polarization degree in these two different situations, we must broaden the acceptance angle in the DLSR and narrow the acceptance angle in the third generation storage ring. The flux in the former case is about 45 times larger than the later case with a same polarization degree of 62% and 52% for HLP and LCP radiation, respectively.

It is worth noting that the interval length between adjacent segments also plays an important role. In the preliminary design, a space of 0.2 m is used to place each phase shifter. The extra diffraction effect at the undulator interval will deteriorate the superposition/counteraction mechanism, as shown in Fig. 8. For the case of a large emittance, the interval length shows a strong effect on reducing the polarization degree. For a small emittance close to the diffraction limit, the dependency on interval length can be significantly relaxed. With the emittance of 100 pm rad, the polarization degrees of HLP and LCP vary slowly, and the maximum polarization degree can reach 93% at zero interval. In contrast, with the emittance of 3 nm rad, a sharp reduction in polarization degree can be observed, and the corresponding maximum values are less than 63% and 52%, respectively.

In practice, unlike the ideal case in which the interval length is ignored, it is no longer possible to make the polarization degree of a third generation storage ring reach a DLSR by reducing the acceptance angle. Figure 9 shows the polarization degree depending on the acceptance angle. There is an upper limit of polarization degree for both the linear and circular mode. In a third generation storage ring, the upper limits of HLP and LCP are approximately 62% and 52%, respectively, while in a DLSR the corresponding upper limit can reach 95%. The DLSR has a higher upper

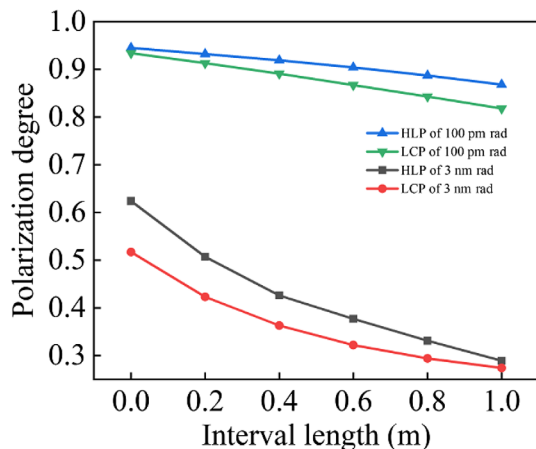


FIG. 8. Polarization degrees (absolute value) of HLP and LCP depend on the interval length within  $1\sigma_p$  for the third generation storage ring and DLSR at 700 eV.

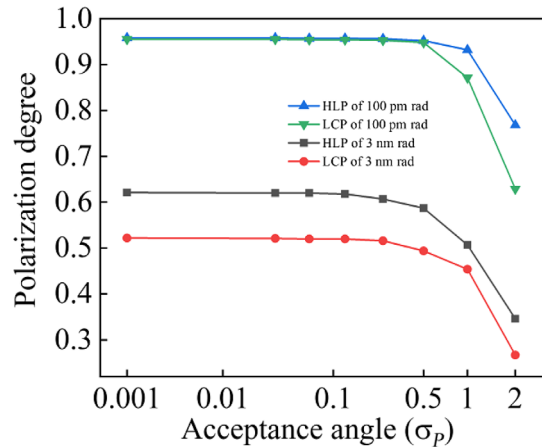


FIG. 9. Polarization degrees (absolute value) of HLP and LCP depend on  $\sigma_p$  for the third generation storage ring and DLSR at 700 eV, with the interval length set to 0.2 m.

limit of polarization degree than a third generation storage ring in this scheme. For a given photon energy and storage ring with the fixed parameters, this upper limit should also be constant. Additionally, the above discussion only considers the influence from emittance. In a typical third generation storage ring, a large beta function will further increase the beam size, then deteriorate the radiation performance. Therefore, for the proposed scheme, a better radiation performance can be expected in a DLSR than in a typical third generation storage ring.

## V. BEAM DEVIATIONS

The superposition/counteraction of undulator radiation is the primary mechanism in the proposed scheme. The longitudinal phase shift is the key to optimizing the polarization feature. Obviously, the transverse mismatch is also important to the proposed scheme. In practice, the field integral can be introduced from each undulator segment and phase shifter. It is possible to cause transverse beam deviation along the undulator, then deteriorate the radiation performance. The beam jitter can also reduce the radiation stability. Next, we will discuss the influence from beam deviation on this scheme. A random beam deviation is assumed. Of course, this deviation should not be too large, otherwise the radiation superposition/counteraction between different segments will be fully destroyed, or the electron beam possibly cannot be maintained in the storage ring.

Based on the electron radiation model in the Appendix, we develop a code to accurately calculate the flux and polarization degree with a small random deviation. The simulation results without beam deviation are consistent with SPECTRA, which validates the effectiveness of the developed code. Then we set two deviation parameters in each segment, including the horizontal deviation and vertical deviation. The deviation parameters are set by random numbers within a certain limit. The circular mode

TABLE II. Average polarization degree, average flux and the corresponding standard deviations under different deviations, in which upper is for the 4-segment scheme and lower is for the 8-segment scheme. The unit of flux and the corresponding standard deviation is ph/(s 0.1% B.W.).

Deviation range	$P_C$	$\sigma(P_C)$	Flux	$\sigma$ (flux)
$0.8\sigma_p$	0.777	0.105	$3.01 \times 10^{14}$	$6.83 \times 10^{13}$
$0.4\sigma_p$	0.925	0.021	$3.51 \times 10^{14}$	$2.64 \times 10^{13}$
$0.2\sigma_p$	0.952	0.005	$3.73 \times 10^{14}$	$7.49 \times 10^{12}$

Deviation range	$P_C$	$\sigma(P_C)$	Flux	$\sigma$ (flux)
$0.8\sigma_p$	0.864	0.071	$2.26 \times 10^{14}$	$4.22 \times 10^{13}$
$0.4\sigma_p$	0.968	0.011	$3.11 \times 10^{14}$	$2.38 \times 10^{13}$
$0.2\sigma_p$	0.985	0.002	$3.59 \times 10^{14}$	$6.88 \times 10^{12}$

for the 4/8-segment scheme is chosen as the example with an acceptance angle of  $1\sigma_p$ . To evaluate the influence only from beam deviation, the interval length is ignored. One hundred groups of calculations for each deviation range are carried out to find the allowed deviation. The radiation performances with the corresponding standard deviations are listed in Table II. At a small deviation range of  $0.2\sigma_p$ , the changes in flux and polarization degree are quite small, thus a good stability can be preserved. With increasing deviation range, the flux and polarization degree decrease, and the corresponding stabilities also become unsatisfactory. Comparing the 8-segment scheme with the 4-segment scheme, we can find that the stability can be further improved by increasing the segment number. For a large segment number, the reduced segment length increases the diffraction angle at each segment. A large diffraction angle then will lower the contribution from beam deviation at each segment. Although the multisegment scheme has high technological difficulty in practice, the superposition/counteraction mechanism can relax the demand on beam deviation to some extent. Actually, in our case, the beam deviation of  $0.2\sigma_p$  is approximately  $4 \mu\text{rad}$ . For a typical third generation storage ring or DLSR, the current technology is able to limit the beam deviation within the micron level, normally equivalent to microradian. The radiation performance influenced by beam deviation in the proposed scheme can be well controlled under the current technology.

## VI. DISCUSSION

### A. Straight section length

Each storage ring light source is characterized by specific beam energy with different straight section length. In the above simulations, the space occupied by phase shifters has been taken into account, but without the practical limitation of straight section length. The length of a standard straight section at HALF is 5.3 m, in which the standard space for insertion device is designed as 4.2 m.

With the 0.2-m-long phase shifter, the total space occupied by the 4/8/16-segment scheme is 3.88/4.68/6.28 m. Under the current limitation for available space of undulator, we do not have enough space to carry on the 8/16-segment scheme. If we keep the same total space (about 4 m) and the same phase shifter length, the period number of each segment should be reduced from 10 to 8 for the 8-segment scheme. Taking the circular mode as an example, in the 8-segment scheme, the flux is  $3.0 \times 10^{14}$  in  $1\sigma_p$  and is  $8.5 \times 10^{14}$  in  $2\sigma_p$ . The corresponding polarization degrees are 97.4% and 91.1%, respectively. Compared with the 4-segment scheme, the polarization degree is always significantly improved while the flux is still considerable. In the 8-segment scheme, the period number of each segment reduced from 10 to 8 only leads to a flux decrease of 32% in  $1\sigma_p$  and 29% in  $2\sigma_p$ . The polarization degree changes little. However, in the 16-segment scheme, the available period number of each segment will be reduced to 1. It cannot work well in this condition.

Actually, it is not difficult to save some space for a specific straight section at HALF. We have kept enough space redundancy for undulator. The 8-segment scheme without reduction of period number (4.68 m) can still be expected to be installed at HALF straight section (5.3 m). In addition, the 0.2-m-long phase shifter is very general in practice, as reported at FLASH and TPS [43,44]. From the aspect of technology, there is still some optimization space to further reduce the phase shifter length. Here we assume to have a small phase shifter with length of 0.1 m, which is a little challenging but still possible to be realized. The 8-segment scheme with 10 periods each segment (3.98 m) can be completely placed at HALF straight section, and the 16-segment scheme with 5 periods each segment (4.78 m) is also possible to be used. Of course, the whole scheme will be very compact. If we still limit the total space of the 16-segment scheme to about 4 m, the period number of each segment should be reduced from 5 to 4. The simulation results show a flux decrease of 29% in  $1\sigma_p$  and 24% in  $2\sigma_p$ , while the polarization degree maintains the same. In this way, the radiation performance is not deteriorated too much in the 16-segment scheme. In fact, some light sources have an ultralong straight section, the space is no longer a noteworthy issue for them. To improve the space utilization in a normal straight section, both the phase shifter length and undulator period length should be reduced.

### B. Issues related to user experiments

For an elliptically polarized undulator, such as APPLE II, the photon energy scan in a small range can be done by only scanning the monochromator, in which the polarization degree or flux does not have a large variation. For the proposed scheme, as indicated in Figs. 2 and 3, the radiation features show a strong relationship with the acceptance angle. The acceptance angle cannot be too large, otherwise the polarization degree will be significantly



reduced, which is not allowed for most of relevant experiments. To work at a large acceptance angle and ensure a high polarization degree in this scheme, the segment number must be increased. In addition, we can observe that the spectrum splits and the polarization degree decreases significantly near the target photon energy. It is indeed an obvious disadvantage of the proposed scheme. During a gap scan the spectral window of monochromator must precisely follow the center photon energy, i.e., undulator gap, to ensure a high polarization degree. Actually, even in a typical APPLE II source, most of the relevant experiments also prefer to scan undulator gap together with the monochromator in a large range of photon energy. Of course, compared with the proposed scheme, the synchronization relationship between monochromator and APPLE II can be relaxed to some extent. Several light sources have developed relevant technologies to solve the synchronization problems, such as the *Turboscan process* developed by SOLEIL [45,46] and a similar technology at SLS [47]. This technology will also be required in the proposed scheme. A good synchronization relationship between undulator gap and monochromator should be calibrated in advance.

For XMLD/XMCD experiments, a stable polarization degree is very important in scanning photon energy. In general, the energy scan range for a certain chemical element is typically around 50 eV and does not exceed 100 eV. In the following we set the energy range to 100 eV and also take the circular mode as an example. The photon energy is selected from 650 to 750 eV. Figure 10 shows the circular polarization degree depending on photon energy at a fixed acceptance angle. The angular divergence  $\sigma_p$  is normalized at 700 eV. With the energy range of 100 eV, the absolute variation of polarization degree is 1.5% in  $1\sigma_p$  and is 6.3% in  $2\sigma_p$  for the 4-segment scheme, while in the 8-segment scheme the variation is 0.4% in  $1\sigma_p$  and is 1.8% in  $2\sigma_p$ . It will be further reduced in the 16-segment scheme.

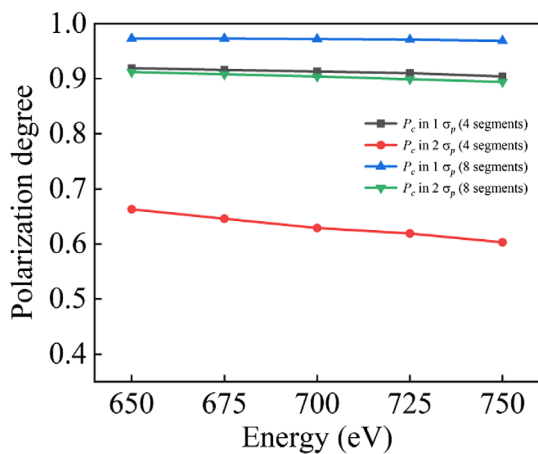


FIG. 10. Polarization degree depends on photon energy at a fixed acceptance angle in the DLSR, with the angular divergence normalizing at 700 eV.

Such a small variation of polarization degree within  $1\sigma_p$  has little influence to user experiments. Within  $2\sigma_p$  of the 4-segment scheme, a slightly large variation can be observed. However, it is approximately linear to photon energy. In relevant experiments, the variation of polarization degree can be compensated by point-to-point precalibration. In addition, as suggested in Sec. V, a large number of segments will be beneficial to improving the tolerance on random beam deviation, which can ensure a stable output in each photon energy. Therefore the polarization stability in the proposed scheme is also possible to satisfy the experimental demand. In a third generation storage ring with a large emittance, the absolute variation is almost the same to a DLSR, but the relative variation is increased.

### C. Switching frequency

Before discussing the switching frequency in this scheme, let us briefly recall the other developed methods [12–19]. The mechanical adjustment of magnet arrays cannot achieve a high switching frequency. The electromagnetic switching of undulator has been demonstrated to achieve the switching frequency of 22 Hz [13]. However, it does not have a good potential to greatly improve the switching frequency. The photon beam line switching is a normal method to achieve the switching frequency as high as the level of kHz, but with different photon beam line and different source point [14,15]. The nature close orbit switching developed recently can achieve the switching frequency of MHz [19]. However, it has different source point and will introduce a heavy disturbance on the beam orbit in other straight sections. The orbit kicker method is developed by SPring-8 with the switching frequency less than 10 Hz [16,33]. The introduced angular or position deviation is typically on the level of hundreds of microradian or on the level of millimetre. The switching frequency is greatly limited by the induced orbit bump and distortion in the storage ring. It manipulates the beam orbit by using several kickers, which is partially similar to the phase shifter method in this paper.

In the proposed scheme, the polarization switching is realized by swapping the phase shifts. Obviously, only the electromagnetic phase shifter has the potential to achieve a fast polarization switching. The unshown simulation confirms that the storage ring is not sensitive to the longitudinal phase shift of electron beam. The orbit bump and distortion induced by phase shifter in the proposed scheme are smaller than the orbit kicker method. Therefore, a high switching frequency can be expected in this scheme. As reported in a similar scheme, the practical switching frequency by swapping electromagnetic phase shifter can reach 13 Hz with only a marginal disturbance of beam orbit [48,49]. The maximum frequency can be expected to 50 Hz. In an electromagnetic phase shifter, the switching frequency more than 100 Hz can be achieved. Through developing the phase shifter combining with the fast kicker

technology, the frequency can even reach 1 kHz. However, the frequency limitation is not only determined by electromagnetic phase shifter itself. A high switching frequency may cause a strong eddy current on the vacuum chamber and affect the electron beam in the storage ring. It is difficult to precisely state that how fast we can successfully achieve until building such an undulator scheme in practice. Nevertheless, we can predict that the switching frequency at least with dozens of Hz is desired to be realized. To further improve the switching frequency, a powerful and accurate switching power supply and a careful examination of eddy current on the chamber will be the preconditions. The chamber material should have a small magnetic permeability and a large resistance. For example, the ceramic vacuum chamber can be used to greatly mitigate the eddy effect. At HALF, the inconel is preliminarily chosen for the vacuum chamber which closes to the fast corrector magnet supplying by the ac power. Additionally, as indicated in Sec. V, a large segment number can improve the tolerance on random beam deviation, so it will relax the demand on beam deviation introduced by phase shifter to some extent in this scheme.

### VII. SUMMARY

In this paper, we simplify and incorporate the previous helical undulator schemes [32,34] to realize fast switching for HLP/VLP and LCP/RCP in the same undulator line. The basic radiation performances are theoretically analyzed and numerically simulated. Furthermore, a large number of undulator segments is demonstrated to be beneficial for improving the radiation performance. Then we compare the scheme in a DLSR and a typical third generation storage ring. Benefiting from the extremely low emittance, the DLSR has a significant advantage in improving the polarization degree or flux under the same polarization degree. When the space occupied by the phase shifter is further taken into account, such difference on radiation performance will be enlarged. The dependency on interval length can be significantly relaxed in a DLSR. An upper limit of polarization degree is demonstrated even with an ultra small acceptance angle. We can conclude that the proposed scheme should have a much better performance in a DLSR than the third generation storage ring.

Currently, the fast development of DLSR significantly reduces the beam emittance, making it possible to rejuvenate segmentally cross-type undulator scheme. Issues that users may particularly concerned have been discussed in details. To carry on an energy scan in this scheme, the photon energy or undulator gap must be calibrated in advance and synchronized with the monochromator. Therefore a lot works should be done associating with the proposed scheme in practice. In addition, increasing the segment number is demonstrated to be beneficial for improving the tolerance on beam deviation and obtaining a stable polarization degree during an energy scan.

However, a large number of segments also will increase the number of phase shifters, synchronically, has a stringent requirement on the length of straight section. In our example, HALF straight section has been used to make a thoughtful discussion. Under the comprehensive development of the storage ring, undulator and phase shifter, it is worthwhile to expect a switching frequency at least with dozens of Hz in this scheme. Swapping the phase shifts will also greatly simplify the following works on optical beam line. Especially, in a DLSR which has a high beam energy and a long straight section, the beam emittance can be further reduced and more undulator segments can be utilized, then the radiation performance of this scheme can be further improved. We hope it can offer a new choice for users to obtain the polarization switching in a DLSR.

### ACKNOWLEDGMENTS

We would like to acknowledge our referees for the helpful comments on the issues related to user experiments and the actual space in a given straight section. We also would like to acknowledge our colleague Kai Chen for meaningful discussion on the requirement of XMLD/XMCD experiments. This work is supported by the National Natural Science Foundation of China under Grants No. 11975233 and No. 11905221 and USTC Research Funds of the Double First-Class Initiative (YD2310002009).

### APPENDIX: ELECTRON RADIATION MODEL

To accurately calculate the photon flux, polarization characteristic and photon beam size, we demonstrate the electron radiation model based on Lienard-Wiechert potential of a point charge. In the far-field approximation, the energy radiated per unit line width, and solid angle, from a single electron passing through the undulator can be calculated by

$$\frac{d^2W}{d\omega d\Omega} = \frac{e^2\omega^2}{4\pi^2c} \left| \int_{-\infty}^{\infty} \mathbf{n} \times (\mathbf{n} \times \boldsymbol{\beta}) e^{i\omega(t-\mathbf{n}\cdot\mathbf{r}/c)} dt \right|^2, \quad (\text{A1})$$

where  $\mathbf{n}$  is the unit vector from the electron position to observation direction,  $\boldsymbol{\beta}$  is the vector of the electron relative velocity,  $\mathbf{r}$  is the unit vector of the position of radiation point. Due to the periodicity of field, the radiation from adjacent period of undulator differs by one given phase, which can be given as

$$\delta = k_s \left( \frac{\lambda_u}{\beta_z} - \lambda_u \cos \theta \right) = \frac{2\pi\omega}{\omega_1(\theta)}. \quad (\text{A2})$$

Benefiting from a constant phase difference, the numerical cost of calculation can be drastically reduced. The radiation characteristics can be calculated from one period. In addition, calculating the total flux radiation from

electron beam should convolute the flux function with the beam density distribution. The optic slit width (or the angular acceptance) should also be included in the calculation. For an electron beam with a standard Gaussian angular distribution (rms width  $\sigma'_e$ ), the angular divergence of the photon beam can be approximately described as

$$\sigma_p = \sqrt{\sigma_e'^2 + \sigma_r'^2}. \quad (\text{A3})$$

Here we limit the discussion to a DLSR, in which  $\sigma'_e$  is much smaller than  $\sigma'_r$ . Thus it is reasonable to replace  $\sigma_p$  by  $\sigma'_r$ . The total flux density from the electron beam with average beam current  $I$  is simplified as

$$\frac{d^2 F}{d\omega d\Omega} = \frac{Ie\omega^2}{16\pi^3\epsilon_0 c} \left| \sum_{m=1}^N e^{i(m-1)\delta} \right|^2 \times \left| \int_{-\lambda_u/2\beta c}^{\lambda_u/2\beta c} \mathbf{n} \times (\mathbf{n} \times \boldsymbol{\beta}) e^{i\omega(t-\mathbf{n}\cdot\mathbf{r}/c)} dt \right|^2. \quad (\text{A4})$$

Combined with the equations of magnetic field, velocity of the electron and the position of the electron below, we can obtain the flux distribution. The magnetic field on the axis can be described as

$$B(z) = \left\{ B_0 \sin\left(\frac{2\pi z}{\lambda_u}\right), B_0 \sin\left(\frac{2\pi z}{\lambda_u} + \phi\right), B_z \right\} \quad (\text{A5})$$

with the velocity and position of electron

$$\boldsymbol{\beta}(t) = \left\{ \begin{array}{l} \frac{\beta_0 K_y}{\gamma} \cos(\omega_0 t), \\ \frac{\beta_0 K_x}{\gamma} \cos(\omega_0 t + \phi), \\ \beta_0 \left\{ 1 - \frac{1}{4\gamma^2} [K_x^2 + K_y^2] \right. \\ \left. - K_y^2 \cos(2\omega_0 t) \right. \\ \left. - K_x^2 \cos(2\omega_0 t + 2\phi) \right\} \end{array} \right\} \quad (\text{A6})$$

$$\mathbf{r}(t) = \left\{ \begin{array}{l} \frac{\beta_0 K_y c}{\omega_0 \gamma} \sin(\omega_0 t), \\ \frac{\beta_0 K_x c}{\omega_0 \gamma} \sin(\omega_0 t + \phi), \\ \beta_0 c \left\{ \left( 1 - \frac{K_x^2 + K_y^2}{4\gamma^2} \right) t \right. \\ \left. - \frac{K_y^2}{8\omega_0 \gamma^2} \sin(2\omega_0 t) \right. \\ \left. - \frac{K_x^2}{8\omega_0 \gamma^2} \sin(2\omega_0 t + 2\phi) \right\} \end{array} \right\}. \quad (\text{A7})$$

With the calculated photon flux, the polarization degrees can be calculated by

$$\begin{aligned} P_L &= \frac{|F_x|^2 - |F_y|^2}{|F_x|^2 + |F_y|^2}, \\ P_C &= \frac{2 \operatorname{Im}(F_x F_y^*)}{|F_x|^2 + |F_y|^2}, \\ P_{45} &= \frac{2 \operatorname{Re}(F_x F_y^*)}{|F_x|^2 + |F_y|^2}. \end{aligned} \quad (\text{A8})$$

The most important issue in the proposed scheme is the superposition/counteraction between radiation fields from different undulator segments. Both the flux and polarization degree are sensitive to this mechanism, thus the transverse deviation of electron beam should be small enough to reduce the mismatch between the undulator radiation. Here we assume an electron beam has a small position deviation ( $\Delta p_d$ ) and a small direction deviation ( $\Delta\theta$ ) before the entrance of the undulator. The new angular radius of the observation angle  $\theta_o$  with respect to the direction deviation is

$$\theta_o = \arctan\left(\frac{L \tan \Delta\theta \pm \Delta p_d}{L}\right) \pm \Delta\theta, \quad (\text{A9})$$

where  $L$  is the distance from the optical source to the observation position and  $\pm$  represents the direction of beam deviation toward the transverse axis.

- 
- [1] S. Sasaki, K. Kakuno, T. Takada, T. Shimada, K.-i. Yanagida, and Y. Miyahara, Design of a new type of planar undulator for generating variably polarized radiation, *Nucl. Instrum. Methods Phys. Res., Sect. A* **331**, 763 (1993).
  - [2] S. Sasaki, Analyses for a planar variably-polarizing undulator, *Nucl. Instrum. Methods Phys. Res., Sect. A* **347**, 83 (1994).
  - [3] A. B. Temnykh, Delta undulator for Cornell energy recovery linac, *Phys. Rev. ST Accel. Beams* **11**, 120702 (2008).
  - [4] T. Schmidt and M. Calvi, APPLE X Undulator for the SwissFEL Soft X-ray Beamline Athos, *Synchrotron Radiat. News* **31**, 35 (2018).
  - [5] X. Liang, M. Calvi, M. E. Couprie, R. Ganter, C. Kittel, N. Sammut, T. Schmidt, M. Valléau, and K. Zhang, Analysis of the first magnetic results of the PSI APPLE X undulators in elliptical polarization, *Nucl. Instrum. Methods Phys. Res., Sect. A* **987**, 164741 (2021).
  - [6] T. Tanaka and H. Kitamura, Figure-8 undulator as an insertion device with linear polarization and low on-axis power density, *Nucl. Instrum. Methods Phys. Res., Sect. A* **364**, 368 (1995).
  - [7] T. Tanaka and H. Kitamura, Analysis of Figure-8-undulator radiation, *J. Synchrotron Radiat.* **3**, 47 (1996).
  - [8] S. Qiao, D. Ma, D. Feng, S. Marks, R. Schlueter, S. Prestemon, and Z. Hussain, Knot undulator to generate linearly polarized photons with low on-axis power density, *Rev. Sci. Instrum.* **80**, 085108 (2009).

- [9] F. Ji, R. Chang, Q. Zhou, W. Zhang, M. Ye, S. Sasaki, and S. Qiao, Design and performance of the APPLE-Knot undulator, *J. Synchrotron Radiat.* **22**, 901 (2015).
- [10] Z. Zhao and Q. Jia, Studies on the asymmetric magnet pole undulators, *Nucl. Instrum. Methods Phys. Res., Sect. A* **999**, 165205 (2021).
- [11] Z. Zhao and Q. Jia, Linearly and circularly polarized radiation with a low on-axis heat load from an asymmetric magnet pole undulator, *Phys. Rev. Accel. Beams* **25**, 050702 (2022).
- [12] T. Tanaka, K. Shirasawa, and H. Kitamura, Consideration on an undulator magnetic structure for polarization control, *Rev. Sci. Instrum.* **73**, 1724 (2002).
- [13] C. Sánchez-Hanke, C. C. Kao, and S. Hulbert, Fast-switching elliptically polarized soft x-ray beamline X13A at NSLS, *Nucl. Instrum. Methods Phys. Res., Sect. A* **608**, 351 (2009).
- [14] K. Sawhney, F. Senf, M. Scheer, F. Schäfers, J. Bahrtdt, A. Gaupp, and W. Gudat, A novel undulator-based PGM beamline for circularly polarised synchrotron radiation at BESSY II, *Nucl. Instrum. Methods Phys. Res., Sect. A* **390**, 395 (1997).
- [15] T. Schmidt, G. Ingold, A. Imhof, B. D. Patterson, L. Patthey, C. Quitmann, C. Schulze-Briese, and R. Abela, Insertion devices at the Swiss Light Source (phase I), *Nucl. Instrum. Methods Phys. Res., Sect. A* **467–468**, 126 (2001).
- [16] T. Hara, K. Shirasawa, M. Takeuchi, T. Seike, Y. Saito, T. Muro, and H. Kitamura, Helicity switching of circularly polarized undulator radiation by local orbit bumps, *Nucl. Instrum. Methods Phys. Res., Sect. A* **498**, 496 (2003).
- [17] J. Cao, Y. Wang, Y. Zou, X. Zhang, Y. Wu, and R. Tai, Optimization of the design for beamline with fast polarization switching elliptically polarized undulators, *J. Synchrotron Radiat.* **23**, 436 (2016).
- [18] K. Tsuchiya, T. Shioya, T. Aoto, K. Harada, T. Obina, M. Sakamaki, and K. Amemiya, Operation of a fast polarization-switching source at the Photon Factory, *J. Phys. Conf. Ser.* **425**, 132017 (2013).
- [19] K. Holldack, C. Schüssler-Langeheine, P. Goslawski *et al.*, Flipping the helicity of X-rays from an undulator at unprecedented speed, *Commun. Phys.* **3**, 61 (2020).
- [20] K. J. Kim, A synchrotron radiation source with arbitrarily adjustable elliptical polarization, *Nucl. Instrum. Methods Phys. Res.* **219**, 425 (1984).
- [21] J. Bahrtdt, A. Gaupp, W. Gudat, M. Mast, K. Molter, W. B. Peatman, M. Scheer, Th. Schroeter, and Ch. Wang, Circularly polarized synchrotron radiation from the crossed undulator at BESSY, *Rev. Sci. Instrum.* **63**, 339 (1992).
- [22] T. Tanaka and H. Kitamura, Improvement of crossed undulator for higher degree of polarization, *AIP Conf. Proc.* **705**, 231 (2004).
- [23] K. J. Kim, Circular polarization with crossed-planar undulators in high-gain FELs, *Nucl. Instrum. Methods Phys. Res., Sect. A* **445**, 329 (2000).
- [24] Y. Ding and Z. Huang, Statistical analysis of crossed undulator for polarization control in a self-amplified spontaneous emission free electron laser, *Phys. Rev. ST Accel. Beams* **11**, 030702 (2008).
- [25] H. Geng, Y. Ding, and Z. Huang, Crossed undulator polarization control for X-ray FELs in the saturation regime, *Nucl. Instrum. Methods Phys. Res., Sect. A* **622**, 276 (2010).
- [26] G. Geloni, V. Kocharyan, and E. Saldin, Improvement of the crossed undulator design for effective circular polarization control in X-ray FELs, in *Proceedings of the FEL2011, Shanghai, China*, pp. 61–64, MOPB25.
- [27] T. Zhang, H. Deng, J. Chen *et al.*, Polarization control proposal for Shanghai deep ultraviolet free electron laser, *Nucl. Instrum. Methods Phys. Res., Sect. A* **680**, 112 (2012).
- [28] H. Deng, T. Zhang, and L. Feng, Polarization switching demonstration using crossed-planar undulators in a seeded free-electron laser, *Phys. Rev. ST Accel. Beams* **17**, 020704 (2014).
- [29] N. Huang, K. Li, and H. Deng, Polarization control of an x-ray free electron laser oscillator, *Phys. Rev. Accel. Beams* **23**, 030702 (2020).
- [30] L. Nahon, M. Corlier, P. Peupardin, F. Marteau, O. Marcouillé, P. Brunelle, C. Alcaraz, and P. Thiry, A versatile electromagnetic planar/helical crossed undulator optimized for the SU5 low energy/high resolution beamline at Super-ACO, *Nucl. Instrum. Methods Phys. Res., Sect. A* **396**, 237 (1997).
- [31] J. Bahrtdt, W. Frentrup, A. Gaupp *et al.*, Elliptically polarizing insertion devices at BESSY II, *Nucl. Instrum. Methods Phys. Res., Sect. A* **467–468**, 21 (2001).
- [32] T. Tanaka and H. Kitamura, Production of linear polarization by segmentation of helical undulator, *Nucl. Instrum. Methods Phys. Res., Sect. A* **490**, 583 (2002).
- [33] S. Yammamoto, Y. Senba, T. Tanaka *et al.*, New soft X-ray beamline BL07LSU at SPring-8, *J. Synchrotron Radiat.* **21**, 352 (2014).
- [34] R. Kinjo and T. Tanaka, Spectrum splitting for fast polarization switching of undulator radiation, *J. Synchrotron Radiat.* **23**, 751 (2016).
- [35] J. Bahrtdt, Shaping Photon Beams with Undulators and Wigglers, in *Synchrotron Light Sources and Free-Electron Lasers: Accelerator Physics, Instrumentation and Science Applications* (Springer, Cham, 2020), pp. 851–933, [https://doi.org/10.1007/978-3-319-04507-8\\_16-3](https://doi.org/10.1007/978-3-319-04507-8_16-3).
- [36] J. Yan, H. Hao, S. Huang *et al.*, Polarization control of a free-electron laser oscillator using helical undulators of opposite helicities, *Phys. Rev. Accel. Beams* **23**, 060702 (2020).
- [37] SPring-8-II conceptual design report, <http://rsc.riken.jp/pdf/SPring-8-II.pdf>.
- [38] Z. T. Zhao, Storage Ring Light Sources, *Rev. Accel. Sci. Technol.* **03**, 57 (2010).
- [39] M. Eriksson, J. F. van der Veen, and C. Quitmann, Diffraction-limited storage rings—a window to the science of tomorrow, *J. Synchrotron Radiat.* **21**, 837 (2014).
- [40] T. Tanaka and H. Kitamura, *SPECTRA*: A synchrotron radiation calculation code, *J. Synchrotron Radiat.* **8**, 1221 (2001).
- [41] L. Wang, Z. H. Bai, N. Hu, H. T. Li *et al.*, Hefei Advanced Light Source: A future soft x-ray diffraction-limited storage ring at NSRL, in *Proceedings of the IPAC2018, Vancouver, BC* (JACoW, Vancouver, BC, Canada, 2018), pp. 4598–4600, THPMK120.

- [42] Z. H. Bai, G. W. Liu, T. L. He *et al.*, A modified hybrid 6BA lattice for the HALF storage ring, in *Proceedings of the IPAC2021, Campinas, SP* (JACoW, Campinas, SP, Brazil, 2021), MOPAB112, pp. 407–409.
- [43] M. Tischer, P. Neumann, A. Schöps *et al.*, Phase shifters for the FLASH2 FEL, in *Proceedings of the IPAC2014, Dresden* (JACoW, Dresden, Germany, 2014), WEPRO032, pp. 2010-2012.
- [44] T.-Y. Chung, C.-S. Yang, Y.-L. Chu, F.-Y. Lin, J.-C. Jan, and C.-S. Hwang, Investigating excitation-dependent and fringe-field effects of electromagnet and permanent-magnet phase shifters for a crossed undulator, *Nucl. Instrum. Methods Phys. Res., Sect. A* **850**, 72 (2017).
- [45] M. Izquierdo, V. Hardion, G. Renaud, L. Chapuis, R. Millet, F. Langlois, F. Marteau, and C. Chauvet, SUMS: Synchronous undulator-monochromator scans at Synchrotron Soleil, *J. Synchrotron Radiat.* **19**, 619 (2012).
- [46] L. Joly, E. Otero, F. Choueikani, F. Marteau, L. Chapuis, and P. Ohresser, Fast continuous energy scan with dynamic coupling of the monochromator and undulator at the DEIMOS beamline, *J. Synchrotron Radiat.* **21**, 502 (2014).
- [47] J. Krempasky, U. Flechsig, T. Korhonen *et al.*, Synchronized monochromator and insertion device energy scans at SLS, *AIP Conf. Proc.*, **1234**, 705 (2010).
- [48] I. Matsuda, A. Kuroda, J. Miyawaki, Y. Kosegawa, S. Yamamoto, T. Seike, T. Bizen, Y. Harada, T. Tanaka, and H. Kitamura, Development of an electromagnetic phase shifter using a pair of cut-core coils for a cross undulator, *Nucl. Instrum. Methods Phys. Res., Sect. A* **767**, 296 (2014).
- [49] J. Miyawaki, S. Yamamoto, Y. Hirata *et al.*, Fast and versatile polarization control of x-ray by segmented cross undulator at SPring-8, *AAPPS Bull.*, **31**, 25 (2021).